Molecular layer perforant path-associated cells contribute to feed-forward inhibition in the adult dentate gyrus

Yan Li[a], Floor J. Stam[b], James B. Aimone[a,1], Martyn Goulding[b], Edward M. Callaway[c], and Fred H. Gage[a,2]

[a]Laboratory of Genetics, [b]Molecular Neurobiology Laboratories, and [c]Systems Neurobiology Laboratories, The Salk Institute for Biological Sciences, La Jolla, CA 92037

Contributed by Fred H. Gage, April 11, 2013 (sent for review February 3, 2013)

New neurons, which have been implicated in pattern separation, are continually generated in the dentate gyrus in the adult hippocampus. Using a genetically modified rabies virus, we demonstrated that molecular layer perforant pathway (MOPP) cells innervated newborn granule neurons in adult mouse brain. Stimulating the perforant pathway resulted in the activation of MOPP cells before the activation of dentate granule neurons. Moreover, activation of MOPP cells by focal uncaging of glutamate induced strong inhibition of granule cells. Together, these results indicate that MOPP cells located in the molecular layer of the dentate gyrus contribute to feed-forward inhibition of granule cells via perforant pathway activation.

adult neurogenesis | interneuron

New neurons, with their distinct excitability and synaptic plasticity, are continually generated from neural progenitor cells and integrate into existing brain circuits throughout adulthood (1). Computational and behavioral evidence has suggested that newly generated dentate granule cells (DGCs) play an important role in memory encoding (2, 3). To further understand the function of newborn neurons in the adult brain, dissection of the circuitry of newborn neurons becomes an important task. We used a genetically modified rabies virus to transsynaptically trace monosynaptic inputs to newborn DGCs (4). This genetically modified rabies virus has recently been used to map neural connectivity in the piriform cortex, amygdala, retinal ganglion cells, and motor neurons (5–9). Unlike traditional tracers, this genetically modified rabies virus is able to target particular cell types and subsequently retrogradely transport across a single synapse, thereby only labeling direct connections onto the initially infected cells (4).

A previous study showed that the development of local inhibitory inputs onto maturing newborn neurons transformed them from a highly excitable to a relatively silent state (10). Local inhibitory circuits in dentate gyrus (DG) are composed of a diverse set of GABAergic interneurons (11). Interneuron networks provide general inhibition to balance excitation and they temporally and spatially regulate the activity of principal neurons (12, 13). The ability to discriminate differences between similar inputs is thought to depend on both feed-back and feed-forward inhibition (FFI), which allows hippocampal neurons to be sensitive to differences of relative input strength in the face of a broad range of overall excitation levels (12, 14).

Different types of interneurons in the hippocampus are typically identified on the basis of firing properties and molecular markers (15). Using the modified rabies virus, we reveal that molecular layer perforant pathway (MOPP) cells are synaptically coupled to newborn granule cells. These MOPP cells have been identified in the molecular layer (ML) of the DG in rat (16), and electron microscopy has revealed that they synapse onto dendritic shafts of spiny and aspiny neurons (17). Here, we provide direct evidence that MOPP cells functionally connect to newborn granule neurons and contribute to FFI in the mouse DG.

Results

Transsynaptic Tracing of the Neural Circuit of Newborn Neurons. We developed a method to extend the utility of a glycoprotein-deleted rabies virus to allow identification of direct synaptic inputs onto newborn neurons (4). First, we engineered a mouse line, $Rosa26^{Lox\text{-}stop\text{-}LoxHTB}$ (HTB: H, histone-tag GFP; T, TVA; B, rabies glycoprotein B19 G), that controls three genes by Cre-recombinase activity: (*i*) histone-tagged GFP (hGFP) to label the nuclei of infected cells; (*ii*) TVA, the avian sarcoma leucosis virus glycoprotein (EnvA) receptor, to allow infection with the EnvA pseudotyped RG-deleted rabies virus [SADdG(EnvA)]; and (*iii*) the rabies glycoprotein B19G (RG) to trans-synaptically and retrogradely spread the virus to presynaptic neurons (Fig. 1*A*). Next, we targeted newborn neurons by utilizing a retroviral vector expressing Cre-recombinase (18). Sequential injection of the Cre retrovirus and SADdG(EnvA) expressing mCherry allowed us to trace monosynaptic inputs onto newborn neurons (Fig.1*B*).

$Rosa26^{Lox\text{-}stop\text{-}LoxHTB}$ mice were injected with Cre-expressing retrovirus followed by rabies injection 3 wk later; the mice were then killed after 1 wk (Fig. 1*C*). We observed three colors of cells: green cells were only infected by retrovirus, yellow cells (hGFP and mCherry expression) were infected by both retrovirus and rabies virus (the starter cells for tracing), and red mCherry-positive cells were presynaptic to the starter cells (Fig. 1*D*). For controls, we either injected retrovirus-expressing GFP (Fig. 1*E*) instead of *cre* recombinase or injected SADdG(EnvA) alone without prior retrovirus injection (Fig. 1*F*). Red cells were not observed in either of these conditions, indicating that SADdG (EnvA) selectively targeted newborn cells and traced their presynaptic inputs. Green and yellow cells were found only in the inner and middle granule cell layer (GCL), consistent with the location of newborn neurons.

First, we analyzed the long-distance connections to newborn neurons. We found red cells in layer II of the ipsilateral entorhinal cortex, which is consistent with the time window of spine and glutamatergic synapse formation in new neurons (19, 20) (Fig. 2*A*). We also found labeled cells in the medial septal nucleus and midbrain (Fig. 2 *B* and *C*). Immunohistochemistry showed that ~70% of red cells in the medial septal nucleus were choline acetyltransferase (ChAT)-positive cells (21) (Fig. 2*B*), suggesting that major inputs from the medial septum to newborn DGCs were cholinergic. Moreover, we found red cells in the midbrain (Fig. 2*C*) near the ventral tegmental area (VTA). Although tyrosine hydroxylase (TH) immunostaining showed the strong signal of dopaminergic neurons

Author contributions: Y.L. designed research; Y.L., F.J.S., and M.G. performed research; Y.L. and J.B.A. analyzed data; and Y.L., E.M.C., and F.H.G. wrote the paper.

The authors declare no conflict of interest.

[1]Present address: Cognitive Modeling Department, Sandia National Laboratories, Albuquerque, NM 87185.

[2]To whom correspondence should be addressed. E-mail: gage@salk.edu.

This article contains supporting information online at www.pnas.org/lookup/suppl/doi:10.1073/pnas.1306912110/-/DCSupplemental.

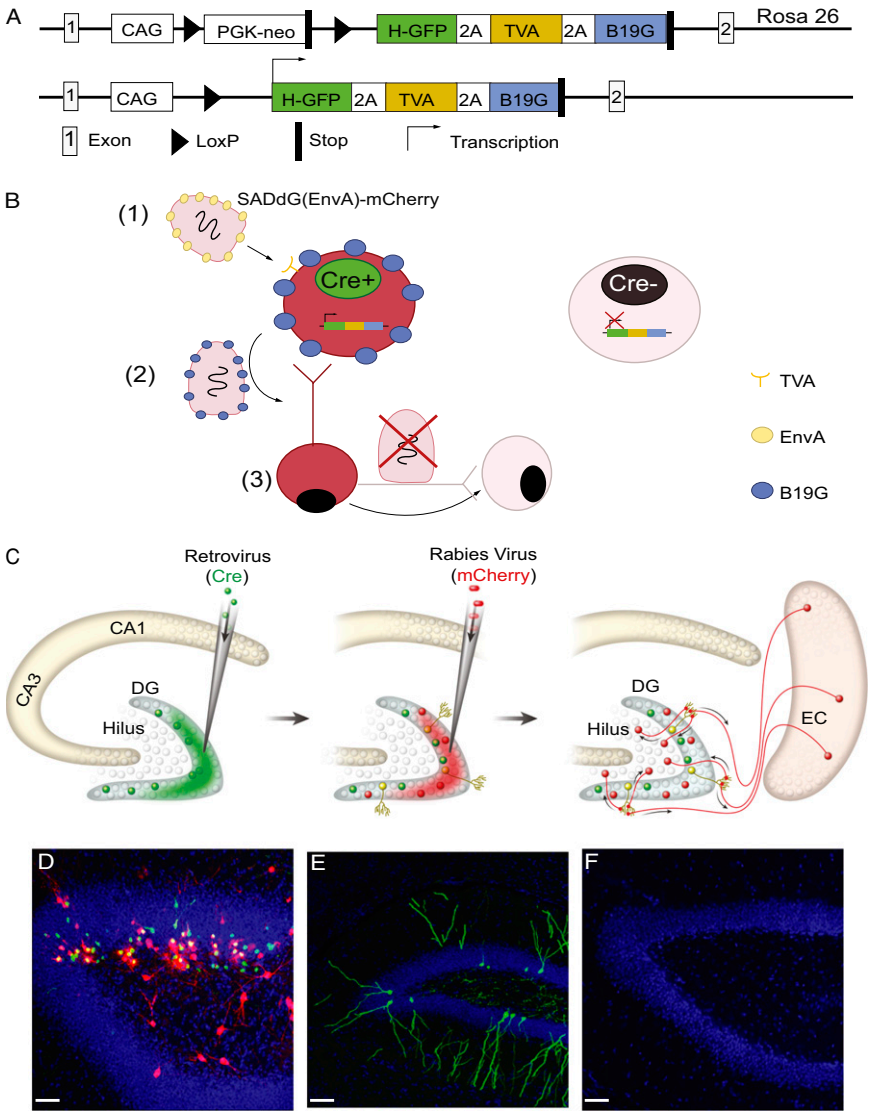

Fig. 1. Schematic representation of mouse line and tracing strategy of monosynaptic inputs to newborn neurons in vivo. (*A*, *Upper*) Schematic representation of the Rosa26$^{LoxP\text{-}stop\text{-}LoxHTB}$ allele used in this study. Coding sequences for hGFP, the TVA receptor and the B19 G rabies glycoprotein are joined by 2A cleavage peptides and preceded by a LoxP flanked stop cassette. (*Lower*) In the presence of Cre recombinase, transcription of the tricistronic ORF is enabled and all three proteins are expressed. (*B*) Schematic representation of the tracing strategy. The recombinant rabies virus, SADdG, has been reported to spread monosynaptically. The glycoprotein gene in SADdG is replaced with fluorescent protein and deletion of glycoprotein in SADdG prevents virus jumping across multiple synapses. Restriction of the initial infection of the rabies virus to a specific neural population is achieved by substituting the glycoprotein of the SADdG rabies virus with an envelope protein from an avian sarcoma and leukosis virus (EnvA) and expressing the highly specific receptor of EnvA, TVA, in a genetically selected population. To use this retrograde-specific tracing system to map the connectivity of newborn neurons, we used the mouse line Rosa26$^{LoxP\text{-}stop\text{-}LoxHTB}$ (1). By delivering Cre-recombinase with a Moloney murine leukemia retrovirus vector, rabies glycoprotein and TVA could be specifically expressed in newborn neurons (2). EnvA-pseudotyped SADdG [SADdG(EnvA)] only infected newborn neurons, and only those newborn neurons could produce rabies virus with the glycoprotein coating necessary to spread to presynaptic neurons (3). Rabies virus stopped at the first connected synapse and could not continue to infect neurons further upstream because the glycoprotein did not exist in the virus or in the upstream neuron's genome. Thus, the combination of retrovirus and rabies virus injections allowed the specific targeting and tracing of the circuitry of adult-born neurons. (*C*) Experimental paradigm. Retrovirus GFP-ires-Cre was injected into the DG of HTB mice. TVA, rabies glycoprotein, and GFP were expressed in newborn neurons labeled in green. Three weeks later, SADdG-mCherry(EnvA) was injected into the same brain region. Rabies virus only infected TVA-expressing newborn neurons, subsequently expressing mCherry and shown in yellow. After 1 wk of SADdG-mCherry (EnvA) injection, the tissue was fixed and visualized with fluorescent microscope. EC, entorhinal cortex. (*D*) DG infected by retrovirus GFP-ires-Cre and SADdG-mCherry(EnvA) injection. Newborn neurons infected by retrovirus alone expressed GFP from retrovirus and transgenic mouse. Neurons infected by both retro- and rabies viruses expressed both GFP and mCherry (yellow cells). Cells infected transsynaptically by rabies virus only expressed mCherry (red cells). (Scale bar: 50 μm.) (*E*) DG infected by retrovirus GFP and SADdG-mCherry (EnvA) injection. Newborn neurons infected by retrovirus and expressed GFP. In the absent of Cre recombinase, TVA was not able to express in newborn neurons, which resulted in no infection by SADdG-mCherry(EnvA). Therefore, only green cells were labeled, but not yellow and red cells. (Scale bar: 50 μm.) (*F*) DG injected with SADdg-mCherry(EnvA) alone. In the absence of retrovirus, rabies virus failed to infect the newborn neuron. Blue represents DAPI signaling. (Scale bar: 50 μm.)

in the VTA, the mCherry-labeled neurons were negative for TH, suggesting that the rabies virus transsynaptic-labeled cells in the midbrain were not themselves dopaminergic.

Next, we examined local circuits in the DG. In the ipsilateral polymorphic layer of the hilus, we found spiny (Fig. 2 *D* and *E*) and aspiny interneurons (Fig. 2*F*). Two types of spiny interneurons

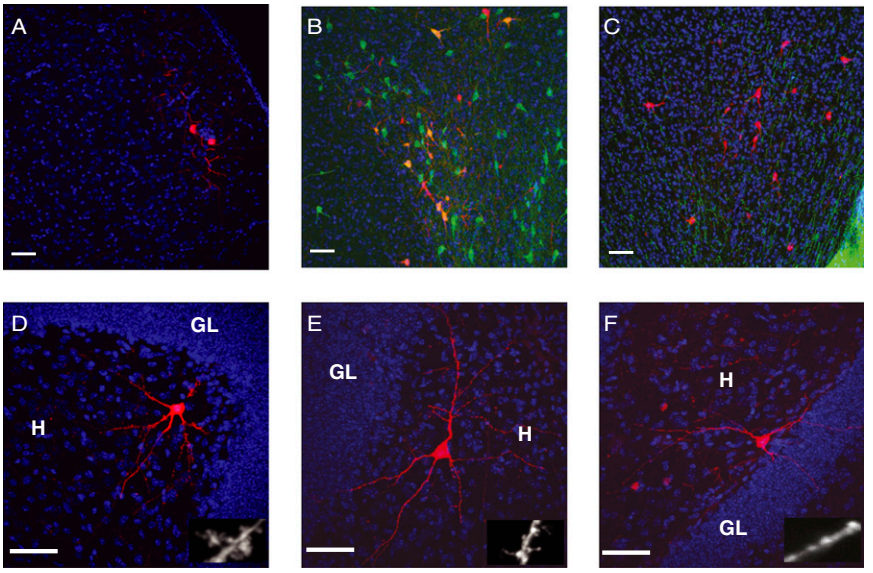

Fig. 2. Monosynaptic inputs to newborn neurons in cortical and subcortical regions and DG. Blue signals represent DAPI staining and the scale bar showed in all figures is 50 μm. GL, granule cell layers. (*A*) Neurons in the ipsilateral entorhinal cortex transsynaptically labeled by SADdG-mCherry(EnvA). (*B*) Neurons labeled in the medial septal nucleus. Red indicates mCherry expression from SADdG-mCherry(EnvA) infection. Green indicates immunofluorescent labeling for ChAT. (*C*) Neurons labeled in the midbrain. Red indicates mCherry expression from SADdG-mCherry(EnvA) infection. Green indicates immunofluorescent labeling for TH. (*D–F*) Neurons labeled in the DG. Mossy cells (*D*), spiny interneuron (*E*), and aspiny interneuron in the hilus (*F*). Higher magnification image of dendrite displayed at right bottom. (Scale bar: *Insets*, 5 μm.

were labeled by rabies virus: one with thorny excrescences, which are the characteristic of Mossy cells (Fig. 2*D*), and another that had thinner and longer spines (Fig. 2*E*) (16). Aspiny neurons are likely basket cells or hilar commissure-associational pathway-related (HICAP) cells (Fig. 2*F*) (16, 22). To further understand the subtypes of cells in DG contacting with newborn neurons, we systematically analyzed the expression of chemical markers of neurons transsynaptically labeled by rabies virus. We found that mCherry-positive cells colocalized with the marker of inhibitory neurons, including calretinin (CR), parvalbumin (PV), and somatostatin (SOM) (Fig. 3), further confirming that newborn neurons receive their inhibitory inputs from the same cell types and regions as mature neurons that are born embryonically (11, 15).

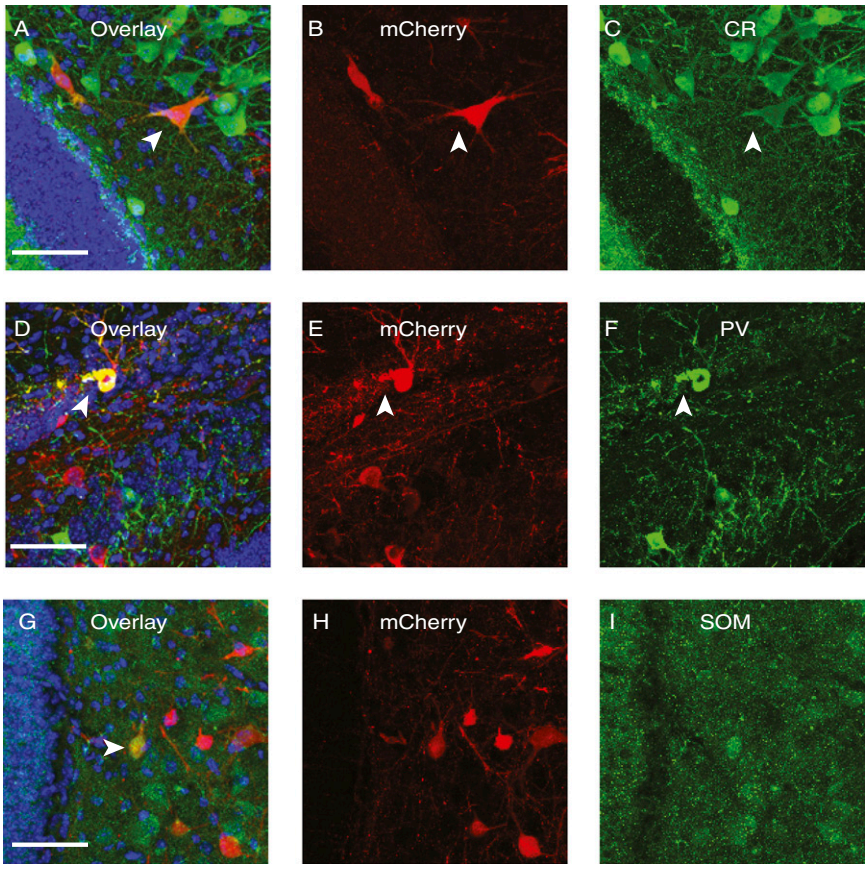

Fig. 3. SADdG-mCherry(EnvA) retrogradely labeled cells in DG expressing interneuron markers. Rabies virus–labeled cells were found colocalized with interneuron markers CR (*A–C*), PV (*D–F*), and SOM (*G–I*). Arrowhead indicates cells with colocalization. Blue represents DAPI signaling. (Scale bar: 50 μm.)

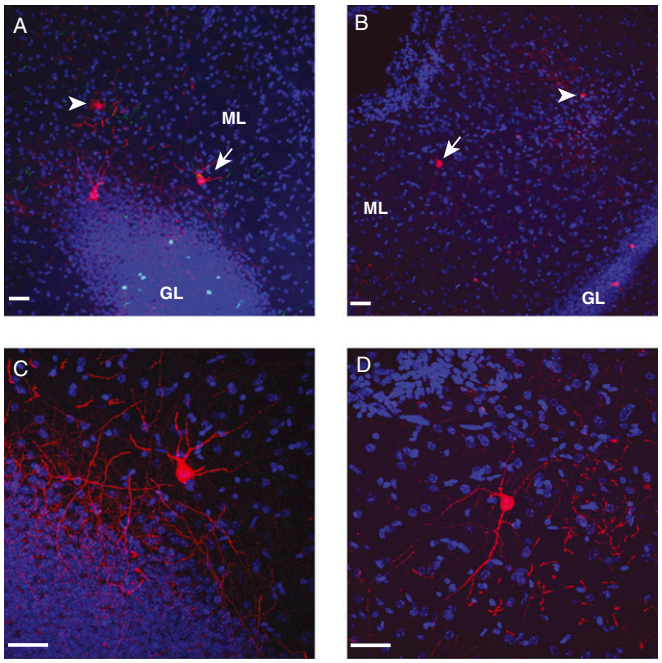

Fig. 4. MOPP cells labeled by rabies virus in the MLs in DG. (*A* and *B*) Neurons (arrows and arrowheads) in the ML of DG transsynaptically labeled by SADdG-mCherry(EnvA). (Scale bar: 50 μm.) (*C* and *D*) Higher magnification image of cells (arrow) in *A* and *B*, respectively. Rabies virus completely fills axons and dendrites of infected neurons with mCherry. Axons of MOPP cells are strictly confined within the ML. No red signals were detected in the subiculum. Blue, DAPI signal. (Scale bar: 50 μm.)

Interestingly, MOPP cells in the inner and outer ML of DG were found traced by rabies virus (Fig. 4 *A* and *B*). MOPP cells had multipolar soma and smooth dendrites and they extended both axons and dendrites into the ML, where projections of neurons in the layer II entorhinal cortex terminate (16, 17). Because the rabies virus completely fills the axons and dendrites of infected neurons with mCherry, it allows us to visualize the detailed morphology of MOPP cells. Outer molecular layer (OML) cells were another cell type found in the MLs in the rat, which had axons that projected across the hippocampal fissure toward the subiculum area (23). It is unlikely that OML cells were labeled because we found that the rabies virus only labeled cells that strictly confined their axons to the ML and we did not see mCherry-labeled axons or cell bodies in the subiculum (Fig. 4 *C* and *D*). Our results suggested that MOPP cells located in the ML were among the presynaptic partners of newborn granule cells. Because MOPP cells were associated with perforant path (PP) terminals, we hypothesized that MOPP cells might be involved in FFI to newborn granule cells.

MOPP Cells in the ML Contribute to FFI. To address our hypothesis, we used conventional electrical stimulation and found that activation of PP was able to drive a disynaptic inhibition onto granule cells (Fig. S1). We then investigated the possibility that MOPP cells were among the local interneurons activated by PP stimulation and providing disynaptic inhibition to DGCs. First we examined whether MOPP cells could functionally innervate DGCs, as suggested by the anatomically retrograde labeling with rabies virus of connections from MOPP cells to DGCs (Fig. 4). To answer this question, we took advantage of focal uncaging of glutamate. This method has been widely used to map the neuronal origins of synaptic connections in cortical networks; we have previously used this approach to characterize the development of inhibitory inputs onto maturing DGCs (10). Whole-cell recordings were obtained from MOPP cells and showed that they exhibited very few spontaneous spikes; however, reliable action potentials were triggered by uncaging glutamate around the cell soma and major dendrites (10). If MOPP cells were functionally connected to granule cells, we would detect inhibitory postsynaptic currents (IPSCs) in granule cells when MOPP cells were activated by locally uncaging glutamate in ML. Because of the refined spatial resolution, even though there are dendrites of PV neurons in the molecular layers, uncaging glutamate in the molecular layer will not activate PV neurons.

We injected a high-titer retrovirus carrying GFP into the DG of 5-wk-old C57 mice. To be consistent with the time window of the rabies virus tracing experiment, acute brain slices were prepared at 3 wk post retrovirus injection. We performed whole-cell recordings in newborn granule cells while holding potential at 0 mV. An example inhibitory input map is shown in Fig. 5*A*. The border of the subregions of DG was drawn in white lines on the map, which was identified under differential interference contrast (DIC) image and confirmed by DAPI staining. The recorded cell was filled with biocytin, and a reconstructed cell with major dendrites is shown in white over the color-coded inhibitory map. The map revealed the pattern and strength of inhibitory inputs to a newborn granule cell under voltage clamp. Photostimulation-induced outward inhibitory currents were recorded when glutamate was uncaged near their presynaptic interneurons (Fig. 5*B*). We measured the amplitude of laser-evoked IPSCs and the number of events following glutamate uncaging at each scanning site. We pooled data from stimulation sites in three different hippocampal regions: ML, GCL, and hilus (H), and then calculated the means for all stimulation sites within each region (10). We found that 3-wk-old DGCs started to receive inhibitory inputs from MLs as well as from hilus and GCL (Fig. 5*C*). The amplitudes of IPSC from ML, GL, and H were 9.75 pA, 9.48 pA, and 7.98 pA, respectively; the numbers of events from ML, GL, and H were 0.48, 0.48, and 0.41, respectively ($n = 8$). Most regions of ML are occupied by the dendritic fibers from

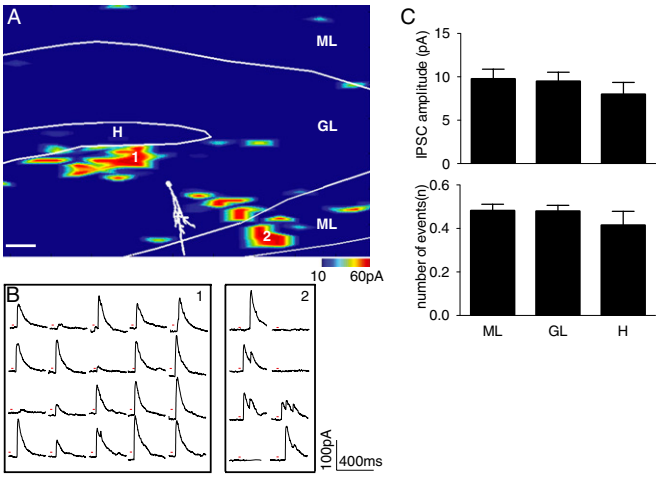

Fig. 5. Inhibitory input from MOPP cells to DGCs identified by laser scanning photostimulation. (*A*) Map of inhibitory input to newborn neuron. A reconstructed cell with soma and major dendrite is shown in white over the pseudocolor input map. The border between the subregions is drawn in a white line on the map. The evoked input strength is shown by a color scale, which represents evoked IPSC amplitudes from 10 to 60 pA. Red range indicates strong inhibitory input; blue indicates weak or no input. (Scale bar: 50 μm.) (*B*) Photostimulation-evoked IPSC traces from areas 1 and 2 are indicated in *A*. Red line at each trace plot indicates the duration of laser. (*C*) Summary of amplitudes of the evoked IPSCs (*Upper*) and numbers of events evoked by photostimulation in each region (*Lower*). Values represent mean ± SEM from eight inhibitory input maps. No statistical difference was detected between regions (one-way ANOVA).

NEUROSCIENCE

DGCs and axonal fibers from entorhinal cortex. Therefore, the functional inputs to newborn neurons detected by photostimulation likely originate from MOPP cells because they are the major cell type identified in the area. Together with rabies virus labeling, our data suggested that MOPP cells were anatomically and functionally connected to newborn DGCs.

We next sought to determine whether MOPP cells were able to receive glutamatergic inputs from PP and generate action potentials by cortical afferent activity. In the presence of the $GABA_A$ receptor blocker, picrotoxin (100 μM), we performed dual patch recordings on newborn DGCs and MOPP cells simultaneously with repetitive PP stimulation (Fig. 6*A*). Biocytin was added to the internal solution and MOPP cells were loaded in whole cell configuration (Fig. 6*B*). For each stimulus strength, the peak excitatory postsynaptic currents (EPSCs) amplitude and firing threshold was measured in pairs of neuron stimulated under the same condition. DGCs had a resting membrane potential of −79.1 ± 1.3 mV and MOPP cells had a resting membrane potential of −63 ± 2.1 ($n = 8$). In voltage clamp mode, EPSCs were evoked from both DGCs and MOPP cells by gradually increasing PP stimulus intensities (0.1–1 mA). Larger amplitudes were recorded in the MOPP cells throughout the entire stimulus range. Two-way ANOVA revealed a significant interaction between cell type and stimulus intensity ($F_{1,8} = 2.243$, $P = 0.027$) and significant effect of cell type ($F_{1,8} = 37.27$, $P < 0.0001$) (Fig. 6*C*). To monitor the firing of MOPP cells and DGCs evoked by excitatory inputs of PP, we recorded cells under the current clamp mode. MOPP cells required about half the synaptic strength as DGCs to fire an action potential ($n = 8$, paired t test $P < 0.001$) (Fig. 6*D*). These findings demonstrated that both MOPP cells and their postsynaptic target DGCs were activated by excitatory inputs from entorhinal cortex and that MOPP cells were preferentially recruited by cortical input activity. Therefore, MOPP cells located in the ML received the excitatory inputs from PP and provided inhibitory input to DGCs, suggesting that MOPP cells are capable of contributing to the FFI.

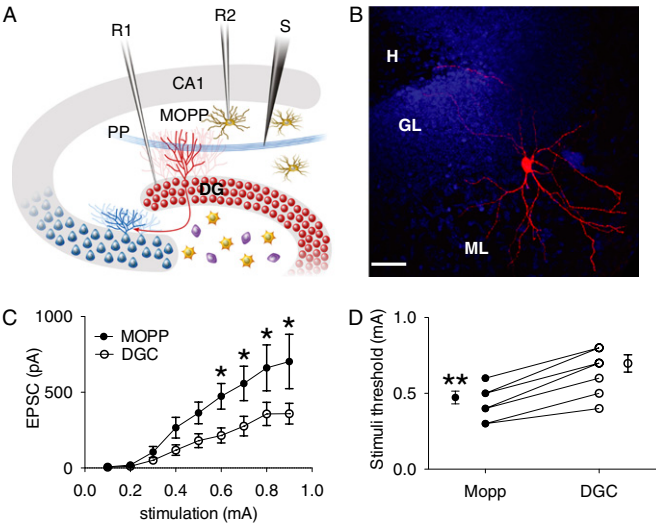

Fig. 6. The activation of MOPP cells by PP stimulation. (*A*) Schematic diagram of dual patch recording configuration. R1 and R2, recording pipettes 1 and 2; S, stimulating electrode. (*B*) Immunofluorescent image of a biocytin-filled MOPP cell in the ML. Blue indicates DAPI staining. (Scale bar: 50 μm.) (*C*) Pairwise analysis of EPSC amplitude vs. stimulus intensity in DGCs and MOPP cells. Whole-cell recordings of MOPP cells and DGCs were obtained under the same condition. The peak amplitudes of EPSC and IPSC were measured in pairs ($n = 9$). *$P < 0.05$ (two-way ANOVA, Bonferroni's post hoc comparison at each stimulation intensity). (*D*) Pairwise analysis of firing thresholds of DGCs and MOPP cells. Spike is measured in whole-cell recording at current clamp mode. Value represents the mean stimulus intensity at which the action potential is consistently generated ($n = 8$). **$P < 0.001$ (paired t test).

Discussion

By combining a genetically modified rabies virus and a retrovirus, we successfully identified the long-distance as well as local inputs to newborn neurons in the adult DG. Because many *cre*-transgenic mice lines are available, this system may be broadly applicable to circuit mapping of other types of neurons. In the future, applying tools that control neural activity into this system will allow functional manipulation of newborn neurons in the circuit (24).

In addition to MOPP cells, HICAP cells and basket cells extend their dendrites into the ML of DG (16), suggesting that PP stimulation might also activate these cells in the H. Therefore, HICAP cells and basket cells, together with MOPP cells, may contribute to FFI to DGG via PP activation. A recently published theoretical model proposed that FFI, acting through MOPP cells, could change the input–output relationship in neuronal information processing (25). During the maturation, the inhibition received by newborn neurons gradually increase. Therefore, young neurons might receive weaker FFI; in response to the same afferent stimulation, FFI might reduce the background firing from mature neurons and facilitate signaling through new neurons. FFI is also likely to contribute to sparse coding in the DG, as has been demonstrated in the olfactory system (26).

Neurogenesis is regulated by many conditions, such as exercise and environmental enrichment, suggesting a role for activity-dependent mechanisms in this process (27–29). At early stages, GABA depolarizes neurons because of high concentrations of intracellular Cl^- (30). Although glutamatergic inputs from entorhinal cortex to newborn neurons are not detected at very early stages (31, 32), cortical afferent activity may still be able to depolarize new neurons through the feed-forward mechanism mediated by interneurons such as MOPP cells. Such a mechanism might allow external cortical inputs to regulate neurogenesis, including neural stem cell proliferation, survival, and differentiation as well as the subsequent integration of the new neurons into the existing neural circuit.

Materials and Methods

Full versions of experimental procedures are presented in *SI Materials and Methods*.

Generation of HTB Transgenic Mice and Animals. The Rosa $26^{Lox\text{-}stop\text{-}LoxHTB}$ (HTB) was generated by cloning a tricistronic open reading frame containing Histone-2B-GFP, TVA and B19 glycoprotein separated by 2A cleavage sequences (HTB) into a Rosa26 targeting vector containing a CAG promoter and a stop signal flanked by LoxP sites.

All experimental procedures followed protocols approved by the Animal Care and Use Committee at The Salk Institute for Biological Studies. All animals were anesthetized with a ketamine/xylazine (100 mg/kg, 10 mg/kg) mixture.

Virus Preparations. All viral production followed the biosafety guidelines approved by the Salk Institute. Moloney murine leukemia retrovirus and the rabies virus were produced as previously described (24, 33).

Slice Preparation and Recording. Brains were transferred to an icy cold cutting solution containing (in mM): 110 choline-Cl^-, 2.5 KCl, 2.0 NaH_2PO_4, 25 $NaHCO_3$, 0.5 $CaCl_2$, 7 $MgCl_2$, 1.3 Na^+-ascorbate, 3.1 Na^+-pyruvate, 20 dextrose, and 4 kynurenic acid (bubbled with 95% O_2 and 5% CO_2). Four hundred micrometer-thick horizontal brain slices were cut in a Vibratome (VT 1000S, Leica) and recovered for 30–60 min in artificial CSF (ACSF) containing (32 °C, in mM): 125 NaCl, 2.5 KCl, 2.0 NaH_2PO_4, 25 $NaHCO_3$, 2.5 $CaCl_2$, 1 $MgCl_2$, 1.3 Na^+-ascorbate, 3.1 Na^+-pyruvate, and 10 dextrose; they were then stored at room temperature. Pipettes for whole-cell recording (pipette resistance, 5–7 MΩ) were filled with internal solution containing the following (in mM): 120 K-gluconate, 15 KCl, 4 $MgCl_2$, 0.1 EGTA, 10 Hepes, 4 MgATP, 0.3 Na_2GTP, and 7 phosphocreatine (pH, 7.2). Biocytin (2 mg/mL) was added to the internal solution for morphological analysis. Patch clamp recordings

were performed at room temperature with an Axopach-200B amplifier (Molecular Devices). Signals were filtered at 2 kHz and sampled at 5 kHz using a Digidata 1320A analog-digital interface (Molecular Devices).

Photostimulation. For the photostimulation experiment, cells were held at a potential of 0 mV to record outward inhibitory current, and potassium in the internal solution was replaced with cesium. 4-methoxy-7-nitroindolinyl-caged-L-glutamate (MNI-caged glutamate, 100 μM, Tocris) was added to recirculating ACSF. UV light (50 mW at 355 nm and 10 mW under the specimen) from an argon-ion laser (Series 3500, DPSS lasers) with 10-ms duration was delivered to brain slices through a 40× microscope objective. More than 800 sites were scanned in a grid with 25 μm of space between the adjacent horizontal and vertical rows. To avoid glutamate receptor desensitization and local caged glutamate depletion, the sequence pattern of laser scanning was designed by computer, which prevented the adjacent site being stimulated within 10 s.

DIC images of brain slices were taken after scanning, and then tissue was fixed in 4% paraformaldehyde (PFA) overnight. Cell morphology was detected by biocytin staining. Overlying the DAPI image with the DIC image was used to establish the position of recording cells and laminar borders of the DG. The border and cells were reconstructed with Neurolucida software (MBF Bioscience). Stimulation sites were aligned to DG subregions by a custom program written in MATLAB (MathWorks).

An inhibitory current map was made by measuring and detecting outward currents of each stimulation site in MiniAnalysis software (Synaptosoft). Events occurring during 10–150 ms after stimulation were counted as synaptic responses. Direct responses evoked by activating glutamate receptors on recorded neurons, which usually occurred within 10 ms after stimulation, were excluded from the analysis. IPSC amplitude and numbers of events at each site were measured by MiniAnalysis. The value at each site was aligned to its layer, and laminar summaries were calculated as the mean response across all stimulation sites within each layer. This method permitted identification of the locations of cell bodies of the neurons that provided synaptic input but could not determine the location of synapses on the dendritic arbor.

Immunohistochemistry. Mice were transcardially perfused by 4% PFA and postfixed overnight, then equilibrated in 30% sucrose. Brain slices were incubated overnight at 4 °C with goat anti-ChAT (1:100, Chemico) and rabbit anti-TH (1:200, Protos Biotech), rabbit anti-parvalbumin (1:1,000, Swant), rabbit anti-calretinin (1:500, Swant), and rabbit anti-somatostatin (1:500, Swant). Cyanine 3- and 5-conjugated secondary antibodies were used against primary antibodies (1:250 Jackson ImmunoResearch). Biocytin signals were detected by cyanine 3-conjugated streptavidin (1:1,000, Jackson ImmunoResearch).

ACKNOWLEDGMENTS. We thank A. Patel and C. Burger for technical assistance, M. L. Gage for editorial comments, and J. Simon for help with illustrations. This work was supported by the Human Frontier Science Program, the James S. McDonnell Foundation, the Mather's Foundation, the National Institute of Mental Health (Grant R01MH063912 to E.M.C.; Grant R37 NS037075 to F.J.S. and M.G.), the Ellison Foundation, and the JPB Foundation (F.H.G.); and by Laboratory Directed Research and Development program support from Sandia National Laboratories (J.B.A.).

1. Zhao C, Deng W, Gage FH (2008) Mechanisms and functional implications of adult neurogenesis. *Cell* 132(4):645–660.
2. Aimone JB, Deng W, Gage FH (2010) Adult neurogenesis: Integrating theories and separating functions. *Trends Cogn Sci* 14(7):325–337.
3. Deng W, Aimone JB, Gage FH (2010) New neurons and new memories: How does adult hippocampal neurogenesis affect learning and memory? *Nat Rev Neurosci* 11(5):339–350.
4. Wickersham IR, et al. (2007) Monosynaptic restriction of transsynaptic tracing from single, genetically targeted neurons. *Neuron* 53(5):639–647.
5. Haubensak W, et al. (2010) Genetic dissection of an amygdala microcircuit that gates conditioned fear. *Nature* 468(7321):270–276.
6. Miyamichi K, et al. (2011) Cortical representations of olfactory input by trans-synaptic tracing. *Nature* 472(7342):191–196.
7. Yonehara K, et al. (2011) Spatially asymmetric reorganization of inhibition establishes a motion-sensitive circuit. *Nature* 469(7330):407–410.
8. Stepien AE, Tripodi M, Arber S (2010) Monosynaptic rabies virus reveals premotor network organization and synaptic specificity of cholinergic partition cells. *Neuron* 68(3):456–472.
9. Vivar C, et al. (2012) Monosynaptic inputs to new neurons in the dentate gyrus. *Nat Commun* 3:1107.
10. Li Y, Aimone JB, Xu X, Callaway EM, Gage FH (2012) Development of GABAergic inputs controls the contribution of maturing neurons to the adult hippocampal network. *Proc Natl Acad Sci USA* 109(11):4290–4295.
11. Houser CR (2007) Interneurons of the dentate gyrus: An overview of cell types, terminal fields and neurochemical identity. *Prog Brain Res* 163:217–232.
12. Kullmann DM (2011) Interneuron networks in the hippocampus. *Curr Opin Neurobiol* 21(5):709–716.
13. Klausberger T, Somogyi P (2008) Neuronal diversity and temporal dynamics: The unity of hippocampal circuit operations. *Science* 321(5885):53–57.
14. Pouille F, Marin-Burgin A, Adesnik H, Atallah BV, Scanziani M (2009) Input normalization by global feedforward inhibition expands cortical dynamic range. *Nat Neurosci* 12(12):1577–1585.
15. Freund TF, Buzsáki G (1996) Interneurons of the hippocampus. *Hippocampus* 6(4): 347–470.
16. Han ZS, Buhl EH, Lörinczi Z, Somogyi P (1993) A high degree of spatial selectivity in the axonal and dendritic domains of physiologically identified local-circuit neurons in the dentate gyrus of the rat hippocampus. *Eur J Neurosci* 5(5):395–410.
17. Halasy K, Somogyi P (1993) Subdivisions in the multiple GABAergic innervation of granule cells in the dentate gyrus of the rat hippocampus. *Eur J Neurosci* 5(5): 411–429.
18. Tashiro A, Sandler VM, Toni N, Zhao C, Gage FH (2006) NMDA-receptor-mediated, cell-specific integration of new neurons in adult dentate gyrus. *Nature* 442(7105): 929–933.
19. Zhao C, Teng EM, Summers RG, Jr., Ming GL, Gage FH (2006) Distinct morphological stages of dentate granule neuron maturation in the adult mouse hippocampus. *J Neurosci* 26(1):3–11.
20. Espósito MS, et al. (2005) Neuronal differentiation in the adult hippocampus recapitulates embryonic development. *J Neurosci* 25(44):10074–10086.
21. Dutar P, Bassant MH, Senut MC, Lamour Y (1995) The septohippocampal pathway: Structure and function of a central cholinergic system. *Physiol Rev* 75(2):393–427.
22. Henze DA, Buzsáki G (2007) Hilar mossy cells: Functional identification and activity in vivo. *Prog Brain Res* 163:199–216.
23. Ceranik K, et al. (1997) A novel type of GABAergic interneuron connecting the input and the output regions of the hippocampus. *J Neurosci* 17(14):5380–5394.
24. Osakada F, et al. (2011) New rabies virus variants for monitoring and manipulating activity and gene expression in defined neural circuits. *Neuron* 71(4):617–631.
25. Ferrante M, Migliore M, Ascoli GA (2009) Feed-forward inhibition as a buffer of the neuronal input-output relation. *Proc Natl Acad Sci USA* 106(42):18004–18009.
26. Assisi C, Stopfer M, Laurent G, Bazhenov M (2007) Adaptive regulation of sparseness by feedforward inhibition. *Nat Neurosci* 10(9):1176–1184.
27. Kempermann G, Kuhn HG, Gage FH (1997) More hippocampal neurons in adult mice living in an enriched environment. *Nature* 386(6624):493–495.
28. van Praag H, Kempermann G, Gage FH (1999) Running increases cell proliferation and neurogenesis in the adult mouse dentate gyrus. *Nat Neurosci* 2(3):266–270.
29. van Praag H, Christie BR, Sejnowski TJ, Gage FH (1999) Running enhances neurogenesis, learning, and long-term potentiation in mice. *Proc Natl Acad Sci USA* 96(23): 13427–13431.
30. Ge S, et al. (2006) GABA regulates synaptic integration of newly generated neurons in the adult brain. *Nature* 439(7076):589–593.
31. Tozuka Y, Fukuda S, Namba T, Seki T, Hisatsune T (2005) GABAergic excitation promotes neuronal differentiation in adult hippocampal progenitor cells. *Neuron* 47(6): 803–815.
32. Deisseroth K, et al. (2004) Excitation-neurogenesis coupling in adult neural stem/progenitor cells. *Neuron* 42(4):535–552.
33. Tashiro A, Zhao C, Gage FH (2006) Retrovirus-mediated single-cell gene knockout technique in adult newborn neurons in vivo. *Nat Protoc* 1(6):3049–3055.